Rare Metal Materials and Engineering
Volume 51, Issue 7, July 2022
Available online at www.rmme.ac.cn

Science Press

Cite this article as: Luo Lei, Duan Ximing, Ma Weijie, et al. Effect of ECAP on Microstructure and Corrosion Resistance Properties of SLM Pure Titanium[J]. Rare Metal Materials and Engineering, 2022, 51(07): 2420-2428.

ARTICLE

Effect of ECAP on Microstructure and Corrosion Resistance Properties of SLM Pure Titanium

Luo Lei[1,2], Duan Ximing[1], Ma Weijie[1], Yang Xirong[1,2], Liu Xiaoyan[1,2], Wang Jingzhong[1,2]

[1] College of Metallurgical Engineering, Xi'an University of Architecture and Technology, Xi'an 710055, China; [2] Shaanxi Key Laboratory of Nanomaterials and Technology, Xi'an 710055, China

Abstract: In order to improve the corrosion resistance of pure titanium in Ringer's simulated body fluid and simulated oral saliva environment, the equal channel angular pressing (ECAP) technique was used to modify the commercial pure titanium prepared by selective laser melting (SLM). The microstructures of SLM pure titanium and SLM+ECAP pure titanium were detected by transmission electron microscope and electron back-scattered diffractometer, and their corrosion resistance was tested by the three-electrode system. Results show that compared with SLM pure titanium, SLM+ECAP pure titanium has smaller grain size, more grain boundaries, higher dislocation density, and modest preferred orientation of the pole diagram with increased pole density. In Ringer's simulated body fluid and simulated oral saliva environment, SLM+ECAP pure titanium has lower self-corrosion current density, higher polarization resistance, and larger impedance radius than SLM pure titanium does. The equivalent circuit fitting of alternating current impedance spectrum was conducted by ZSimpWin software, and the fitting results are in good agreement with the experiment data. The corrosion resistance of SLM+ECAP pure titanium is better than that of SLM pure titanium.

Key words: equal channel angular pressing; selective laser melting; pure titanium; corrosion resistance property

As a rare metal, titanium is often used as human implant in clinic because of its low elastic modulus, good biocompatibility, and high stability. In the dentistry field, titanium is widely applied in crown and bridge prosthesis, dental implant, denture bracket, orthodontic arch wire, implant abutment, titanium plate, titanium nails, and orthodontic anchor nails[1-3]. In the orthopedics field, titanium has also become one of the preferred materials for human limb (hip, knee, ankle, shoulder, elbow, wrist, finger joint), bone bonding products, bone trauma products (screws, plates, intramedullary nails), and spinal internal fixation system implants[4-6]. However, due to the restrictions of traditional manufacture techniques, the personalized and targeted needs of titanium implants are hard to satisfy in biomedical field.

The selective laser melting (SLM) technique can accurately produce the 3D objects, therefore easily obtaining the personalized, integrated, and functional complex structures[7,8]. Many materials have been applied through SLM, such as steel[9,10], aluminum[11-13], titanium[14], nickel[15,16], and their related alloys. However, due to the aggravation of aging population and the frequent occurrence of accidents, the demand for human implants in the medical filed is increasing. When the biomaterials are implanted into the human body, the corrosion will occur in the complex human environment containing various inorganic ions (Na^+, Cl^-, K^+), thereby affecting the protein, nucleic acid metabolites, and enzymes in human body. The corrosion products and metal ions can stimulate the normal tissues of the human body and result in infection, distortion, and other issues. Therefore, the metal implants should have a semi-permanent or permanent service lifetime. The metal artificial joint has semi-permanent service lifetime, i.e., it can be used in human body for more than 15 a. In such a long period of time, the implants in the complex body fluid environment not only are affected by the periodic external forces, but also suffer the consistent corrosion. Therefore, the requirements for the corrosion resistance of biomaterials are higher.

It is known that the severe plastic deformation (SPD)

Received date: July 01, 2021
Foundation item: National Natural Science Foundation of China (51474170); Foundation of Shaanxi Key Laboratory of Nanomaterials and Technology; Natural Science Special Fund of Xi'an University of Architecture and Technology (ZR19043)
Corresponding author: Luo Lei, Ph. D., Associate Professor, College of Metallurgical Engineering, Xi'an University of Architecture and Technology, Xi'an 710055, P. R. China, E-mail: luolei@xauat.edu.cn

process can improve the corrosion resistance of metal materials, and it can produce titanium-based dental and orthopedic implants[17]. The fine titanium used for implant has higher fitting degree and faster healing process, and therefore can reduce the risk of rapid loss of stability after implantation. The equal channel angular pressing (ECAP), as one of SPD methods, can improve the corrosion resistance of metal materials without changing the cross-section shape and area of the objects, thereby attracting great attention. Balakrishnan et al[18] studied the corrosion resistance of ultrafine titanium through Tafel curves, and found that the corrosion resistance of ultrafine titanium prepared by ECAP process is 10 times better than that of original pure titanium in the simulated body fluid (SBF). Irfan et al[19] prepared the CP-Ti material of nanostructure by four-pass ECAP at high temperature (400 ° C), and evaluated its corrosion resistance and wear resistance in SBF by mass loss measurement. It is found that ECAP process can improve the corrosion resistance and wear resistance of CP-Ti material.

Although ECAP has been commonly used in the processing of titanium and titanium alloys, the pure titanium manufactured by additive manufacturing (AM) is rarely treated by ECAP and its application in biomedicine is rarely reported. This research revealed the influence of ECAP on the corrosion resistance of pure Ti after SLM, providing a solid theoretical foundation for the improvement of the corrosion resistance of pure titanium implants. Thus, this research provides guidance for the clinical application of pure titanium implants in surgical operation.

1 Experiment

The raw material used in the experiment was spherical CP-Ti powder prepared by the induction gas atomization process without crucible electrode (TLS company, Germany). The powder composition is shown in Table 1, which meets the requirements of GB/T 13810-2007[20] and ASTM F67-2006a[21].

Pure titanium bar with the size of Φ20 mm was prepared by SLM 125HL 3D printer. The argon gas of 99.9vol% was used as protective gas, and the scanning method was layer-by-layer alternate scanning. A bar-shaped specimen with a size of Φ20 mm×200 mm was cut by the wire cutting, and then a die with the channel included angle φ=120° and an external fillet angle ψ =20° was used for single ECAP extrusion at room temperature by a four-column hydraulic press of YJ32-160B model. The extrusion speed was 2.5 mm·s^{-1}, and a self-made lubricant with MoS_2 and graphite as the main components was used to reduce the friction between the deformed specimen and the mold. The JEM-200CX transmission electron microscope (TEM) and the NORDLYS NANO electron back-scattered diffractometer (EBSD) were used to test the microstructure and pole figure of the specimens before and after ECAP. The schematic diagram of specimens is shown in Fig. 1, and the test surface is the extrusion direction (ED) surface of the specimens. The test position is at the center position of the specimen. ND and TD represent the normal direction and transverse direction, respectively.

The block test specimen was cut into the one with size of 10 mm×10 mm×5 mm. Firstly, the specimen was roughly ground, and then a copper wire was welded on the back of the test specimen to ensure the good conductivity between the test surface and the tail end of the copper wire. Then, the specimen was embedded in the plastic tube with denture base resin and denture powder. The exposed area was 1 cm^2. Finally, the specimen was ground, polished, cleaned, and dried.

The three-electrode system was used: the prepared specimen was the working electrode (WE), the platinum electrode was the auxiliary electrode (AE), and the saturated calomel electrode (SCE) was the reference electrode (RE). The corrosion environments were Ringer's SBF and simulated oral saliva, and their composition is shown in Table 2 and Table 3, respectively. During the test, the corrosion solution was placed in the water bath at 37 ℃, and the pH value of the corrosion solution was 7.2.

The open circuit potential curve, polarization curve, and alternate current (AC) impedance spectrum of specimens were obtained. The duration of the open circuit potential curve measurement was 3600 s, and the sampling interval of the

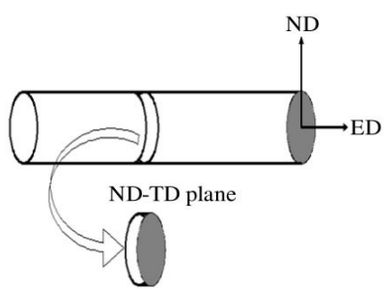

Fig.1 Schematic diagram of specimen and ED test surface

Table 1 Composition of CP-Ti powder used in experiment and in ASTM F67-2006a and GB/T 13810-2007 standards (wt%)

Composition	C	H	N	O	Fe	Ti
CP-Ti powder	0.004	0.0015	0.005	0.088	0.030	Bal.
ASTM F67-2006a	<0.08	<0.015	<0.03	<0.18	<0.20	Bal.
GB/T 13810-2007	0.10	0.015	0.03	0.20	0.25	Bal.

Table 2 Chemical composition of Ringer's SBF

NaCl	$NaHCO_3$	$CaCl_2·6H_2O$	KCl	H_2O
9 g	0.2 g	0.25 g	0.4 g	1 L

Table 3 Chemical composition of simulated oral saliva (g)

KCl	NaCl	$CaCl_2·2H_2O$	KH_2PO_4	K_2HPO_4	$MgCl_2·H_2O$	Peptone
1.3	0.1	0.1	0.027	0.035	0.05	0.5

specimen was 0.5 s. The starting and ending potentials of the polarization curve were −2~2 V, the scanning rate was 0.05 V/s, the waiting time was 10 s, and the sampling interval was 0.001 s. The frequency range of AC impedance spectrum was 100 kHz~10 mHz, the amplitude of sinusoidal AC wave was 10 mV, and the waiting time was 10 s. Finally, the ZSimpWin software was used to fit and analyze the data in AC impedance spectrum.

2 Results

2.1 Microstructure evolution

Fig.2 shows the microstructures of SLM pure Ti and SLM+ECAP pure Ti by optical microscope (OM). It can be seen from Fig. 2 that after ECAP treatment, the Ti structure is subjected to severe shear deformation and extrusion, the grains are broken, and the grain boundaries are increased, resulting in the refinement of original coarse grains.

Fig. 3 shows the bright field TEM images of SLM pure Ti and SLM+ECAP pure Ti. It can be seen that the grain size of SLM pure Ti specimen is large, the grain boundary is clear (as indicated by the arrow in Fig. 3a), and there are uneven dislocation lines in the grain (as indicated by the arrows in Fig. 3b). The SLM+ECAP pure Ti specimen has more grain boundaries, the dislocation density increases, and the dislocations are intertwined to form more dislocation entanglement areas. During ECAP deformation, the dislocation rearrangement and elimination cause the dynamic recovery, leading to the fact that the dislocation entanglement area gradually evolves into many dislocation cells. The increase in dislocation density may be due to the fact that when the SLM pure Ti specimen is deformed by the external force, the shear stresses between the grains with different orientations are different. During the coordination process of grains with different orientations, the slip occurs in the grains with soft orientation preferentially and then in the grains with hard orientation. Different passes of ECAP deformation lead to the non-uniformity of deformation, which in turn increases the dislocation density. Fig. 4 shows the {0002}, $\{11\bar{2}0\}$, and $\{10\bar{1}0\}$ pole figures of SLM pure Ti and SLM+ECAP pure Ti. It can be seen that the maximum pole density of SLM pure Ti specimen is 6.10. The {0002} polar figure has obviously preferred orientation, and its *C* axis is approximately parallel

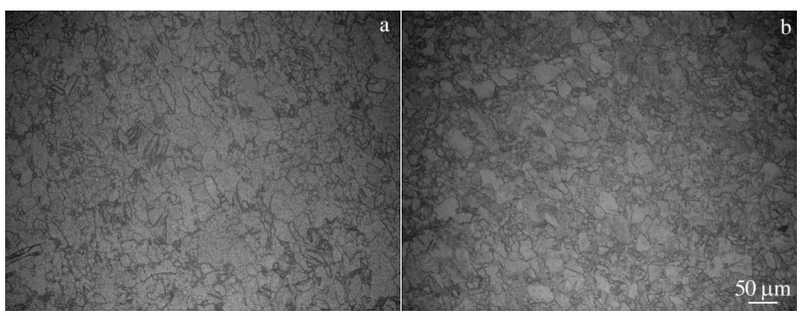

Fig.2 OM microstructures of SLM pure Ti (a) and SLM+ECAP pure Ti (b)

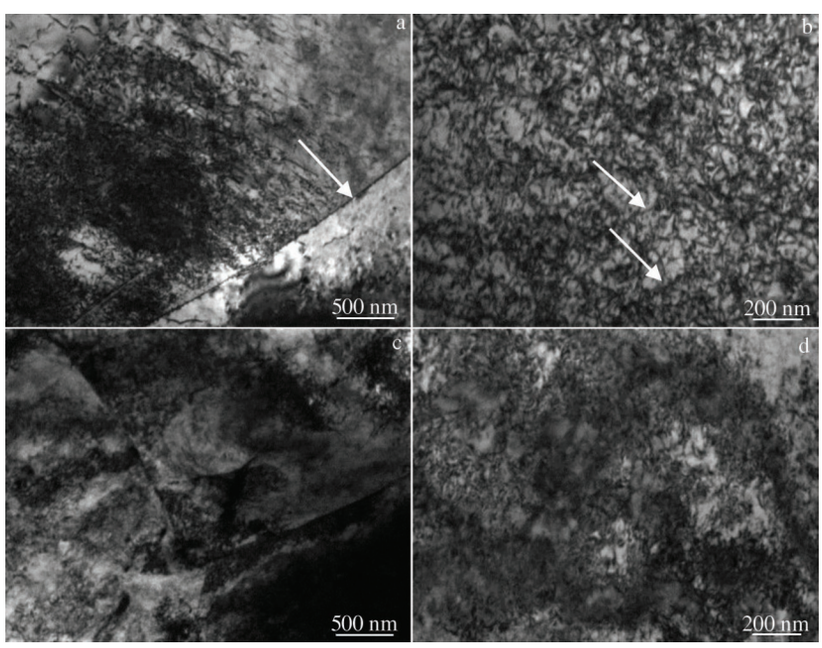

Fig.3 TEM microstructures of SLM pure Ti (a, b) and SLM+ECAP pure Ti (c, d)

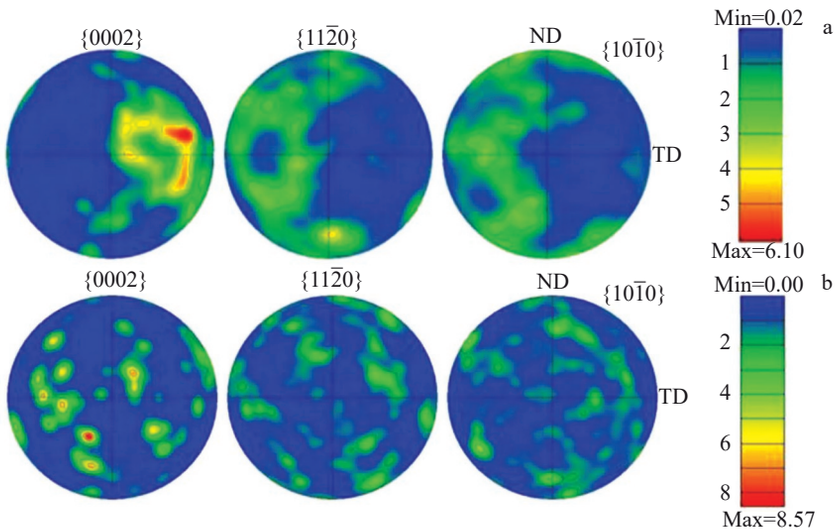

Fig.4 Pole figures of SLM pure Ti (a) and SLM+ECAP pure Ti (b)

to TD. The {11$\bar{2}$0} pole figure has a relatively weak pole, whose orientation is parallel to ND. Due to the effect of shear deformation, the maximum pole density of SLM+ECAP pure Ti is 8.57. Compared with those of SLM pure Ti, the points with high pole intensity in the {0002} pole figure are along ND and TD, and the preferred orientation is not obvious. Besides, more points with sub-high pole intensity can be observed due to the twins. After one-pass of ECAP, the points with high pole intensity are scattered in the pole figures of the pure Ti.

2.2 Corrosion resistance

2.2.1 Corrosion resistance of pure Ti in Ringer's SBF

Fig. 5 shows the open circuit potential curves of SLM pure Ti and SLM+ECAP pure Ti specimens in Ringer's SBF. It can be seen from Fig. 5 that the open circuit potentials of the two specimens are firstly decreased and then stabilized. During the entire immersion process, the open circuit potential of the SLM+ECAP pure Ti is higher than that of the SLM pure Ti, and it reaches the stabilization earlier. At the initial stage of the immersion, the potential of SLM+ECAP pure Ti is higher than that of the SLM pure Ti, indicating that its oxide film is relatively more completed. With the test proceeding, the potential is decreased, indicating that the dissolution rate is greater than the formation rate, i. e., the oxide film is dissolving. After 1500 s, the open circuit potential of the SLM+ECAP pure Ti is basically stabilized with a slight potential rise. These phenomena all infer that the electrochemical activity of the SLM+ECAP pure Ti is very strong in the initial corrosion stage, and then the dissolution and formation of the relatively stable passive film reach a dynamic balance. The open circuit potential of SLM+ECAP pure Ti is more positive, which indicates that its corrosion sensitivity is low, its passive film is relatively stable, and its surface performance is excellent. Thus, the corrosion can hardly occur in SLM+ECAP pure Ti. The mechanism of the enhanced corrosion resistance of SLM+ECAP pure Ti is that the SLM+ECAP pure Ti has more grain boundaries, which reduces the segregation impurities at grain boundaries and increases the channels for atom diffusion. As a result, the formation efficiency of passive film is increased and the surface electrode potential is uniform.

Fig. 6 shows the potentiodynamic polarization curves of SLM pure Ti and SLM+ECAP pure Ti after immersion in Ringer's SBF for 1 h. The shapes of the activation zone,

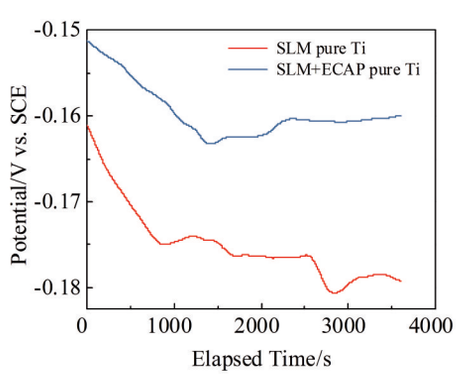

Fig.5 Open circuit potential curves of SLM pure Ti and SLM+ECAP pure Ti in Ringer's SBF

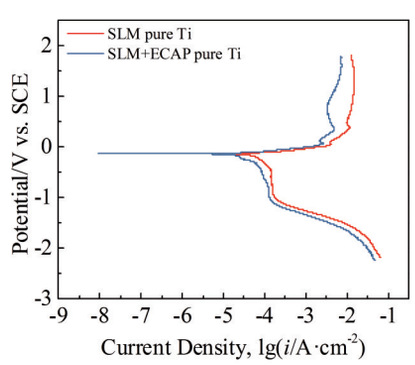

Fig.6 Potentiodynamic polarization curves of SLM pure Ti and SLM+ECAP pure Ti in Ringer's SBF

strong polarization zone, and cathode polarization zone of the two curves are similar, which indicates that the corrosion mechanisms of these two specimens are also similar.

In the process of anodic polarization, the current density of SLM+ECAP pure Ti and SLM pure Ti increases abruptly at 0.04 and 0.06 V vs. SCE and at 0.38 and 0.40 V vs. SCE, respectively, indicating the unstable passive film, local rupture, and pitting corrosion. With increasing the current density, the potential of SLM+ECAP pure Ti and SLM pure Ti enters the passivation zone at 1.1 and 0.8 V vs. SCE, respectively. Thereafter, the current density is basically stable as the electrode potential moves rapidly along the positive direction, suggesting that the formation of passive film on the Ti surface is faster than the dissolution of passive film. Thus, the pure Ti specimen is passivated.

It can be seen from Table 4 that although the self-corrosion potential (E_{corr}) of SLM+ECAP pure Ti is similar to that of SLM pure Ti, the self-corrosion current density (i_{corr}) of SLM+ECAP pure Ti is smaller and its polarization resistance (R_p) is larger, compared with those of SLM pure Ti. The smaller the corrosion rate, the better the corrosion resistance of the oxide film on Ti surface. Thus, the corrosion resistance of SLM+ECAP pure Ti is better than that of SLM pure Ti.

Fig.7 shows the Nyquist plots and Bode plots of SLM pure Ti and SLM+ECAP pure Ti in Ringer's SBF. It can be seen from Fig.7a that the impedance radius of SLM+ECAP pure Ti is obviously larger than that of SLM pure Ti. The larger the radius of the semicircle, the larger the values of Z' and Z'', i.e., the greater the impedance, the better the corrosion resistance of pure Ti.

The curves of the absolute value of impedance at low frequency is shown in Fig. 7b. The straight lines can be observed in the low and medium frequency range in Fig. 7b, which represents the existence of Warburg impedance. When the Warburg phenomenon occurs, the dominated corrosion mechanism changes from the electrochemical reaction into the ion diffusion and transfer. The larger the Warburg impedance, the worse the conductivity, the less the charge on the electrode surface, and the slower the corrosion rate.

It can be seen from Fig. 7c that the phase angles of SLM+ECAP pure Ti and SLM pure Ti are both about 20° in the low and high frequency regions. In addition, the phase angles of these two Ti specimens in the middle frequency region are similar, both more than 60°, but the intermediate frequency range of the SLM+ECAP pure Ti is obviously wider. According to the Tafel curves, it is shown that the wider the platform of the intermediate frequency region as well as the larger the maximum phase angle, the slower the corrosion rate of electrode.

Currently, the research of AC impedance spectroscopy is mainly based on the equivalent circuit simulation. Through the analysis of AC impedance spectrum, it is found that the curve deviates from the semicircle, indicating that the dispersion effect occurs. This may be related to the electrochemical inhomogeneity of the working electrode surface and the conductivity of the adsorption layer and the solution around the electrode surface. Therefore, the electric double layer at the electrode interface cannot be equivalent to a capacitor, and the equivalent circuit with constant phase-angle element (CPE) can be well fitted for the AC impedance spectrum with dispersion effect.

By ZSimpWin software, the electrochemical impedance spectrum (EIS) curves of SLM pure Ti and SLM+ECAP pure Ti were fitted and analyzed, and the equivalent circuit is shown in Fig. 8. R_1 is the solution resistance between the Luggin capillary of RE and WE; R_2 is the charge transfer resistance (passive film resistance), which can directly characterize the corrosion resistance of the material; CPE_1 reflects the ability of the material to accumulate charge; W_1 represents the Warburg effect. The fitting results are listed in Table 5, and they are in good agreement with the experiment results in Fig.9, showing the prediction accuracy.

As shown in Table 5, the solution resistance R_1 is smaller than that of the passive film resistance R_2, the charge

Table 4 Corrosion resistance properties of SLM pure Ti and SLM+ECAP pure Ti specimens in Ringer's SBF

Specimen	E_{corr}/ V vs. SCE	i_{corr}/ $\times10^{-5}$ A·cm^{-2}	R_p/Ω·cm^2
SLM pure Ti	−0.143 29	4.455 2	404.03
SLM+ECAP pure Ti	−0.140 25	1.851 8	972.04

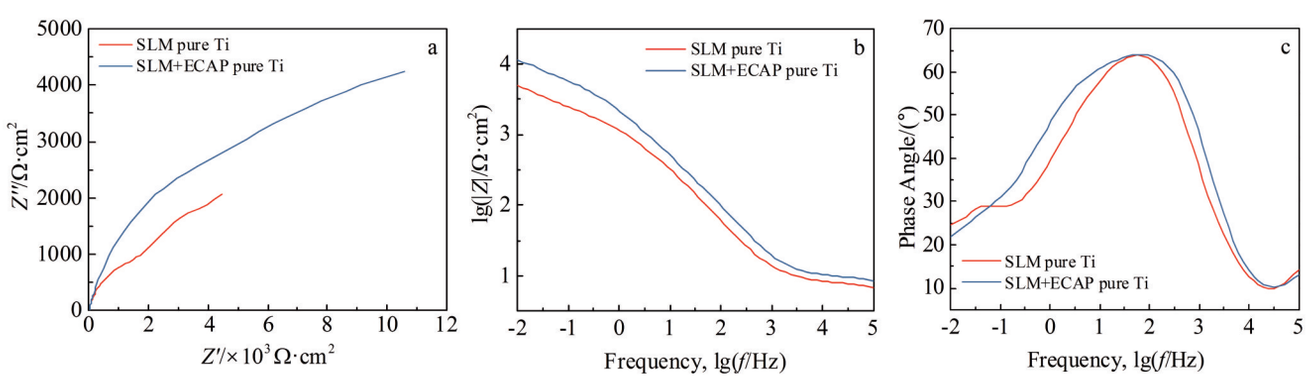

Fig.7 Nyquist plots (a), impedance-frequency plots (b), and phase angle-frequency plots (c) of SLM pure Ti and SLM+ECAP pure Ti in Ringer's SBF

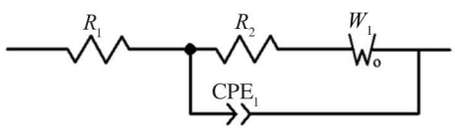

Fig.8 Schematic diagram of EIS equivalent circuit of SLM pure Ti and SLM+ECAP pure Ti in Ringer's solution

accumulation ability of SLM+ECAP pure Ti specimen is inferior to that of SLM pure Ti specimen according to the CPE values, and the fitting parameter n is a CPE_1 index related to surface roughness and defects, whose size can usually reflect the uniformity of passive film. It is found that the n values of SLM pure Ti and SLM+ECAP pure Ti are similar, indicating that there is little difference in the uniformity of passive film between these two Ti specimens. Whereas the values of passive film resistance R_2 and Warburg impedance W_1 of SLM+ECAP pure Ti are higher than those of SLM pure Ti, indicating that the charge transfer between the medium and electrode is more difficult for SLM+ECAP pure Ti. Thus, the corrosion resistance of SLM+ECAP pure Ti is better, which is consistent with the results of potentiodynamic polarization curves.

2.2.2 Corrosion resistance of pure Ti in simulated oral saliva

Fig.10 shows the open circuit potential curves of SLM pure Ti and SLM+ECAP pure Ti in the simulated oral saliva. It can be seen that the open circuit potential of SLM pure Ti is more and more negative, and finally reaches −0.0445 V vs. SCE after 3600 s. The initial open circuit potential of SLM pure Ti is higher than that of SLM+ECAP pure Ti, suggesting that the passive film of SLM pure Ti is relatively completed. However, with the immersion process proceeding, the potential of SLM pure Ti is decreased rapidly, indicating that the electrochemical activity of SLM pure Ti is stronger, and the formation rate of passive film is slower than dissolution rate of passive film. The open circuit potential of SLM+ECAP pure Ti increases slowly at first and then decreases gradually, which may be affected by the dissolution and formation of passive film. In the initial corrosion stage, the increase in potential indicates the gradually weakened electrochemical activity of SLM+ECAP pure Ti, which is caused by the corrosion product film covered on the electrode surface, and the passive film is continuously formed. After 1200 s, the open circuit potential gradually decreases, indicating that the passive film starts to dissolve.

Fig.11 shows the potential polarization curves of SLM pure Ti and SLM+ECAP pure Ti during immersion in simulated

Table 5 Simulated EIS results of SLM pure Ti and SLM+ECAP pure Ti specimens in Ringer's SBF

Specimen	R_1/Ω·cm^2	CPE_1/Ω^{-1}·cm^{-2}·s^n	n	R_2/Ω·cm^2	W_1/Ω^{-1}·cm^{-2}·s$^{0.5}$
SLM pure Ti	7.480	1.0897×10^{-4}	0.777 90	987.6	0.122 98
SLM+ECAP pure Ti	8.825	7.1563×10^{-5}	0.785 76	1100.0	0.178 11

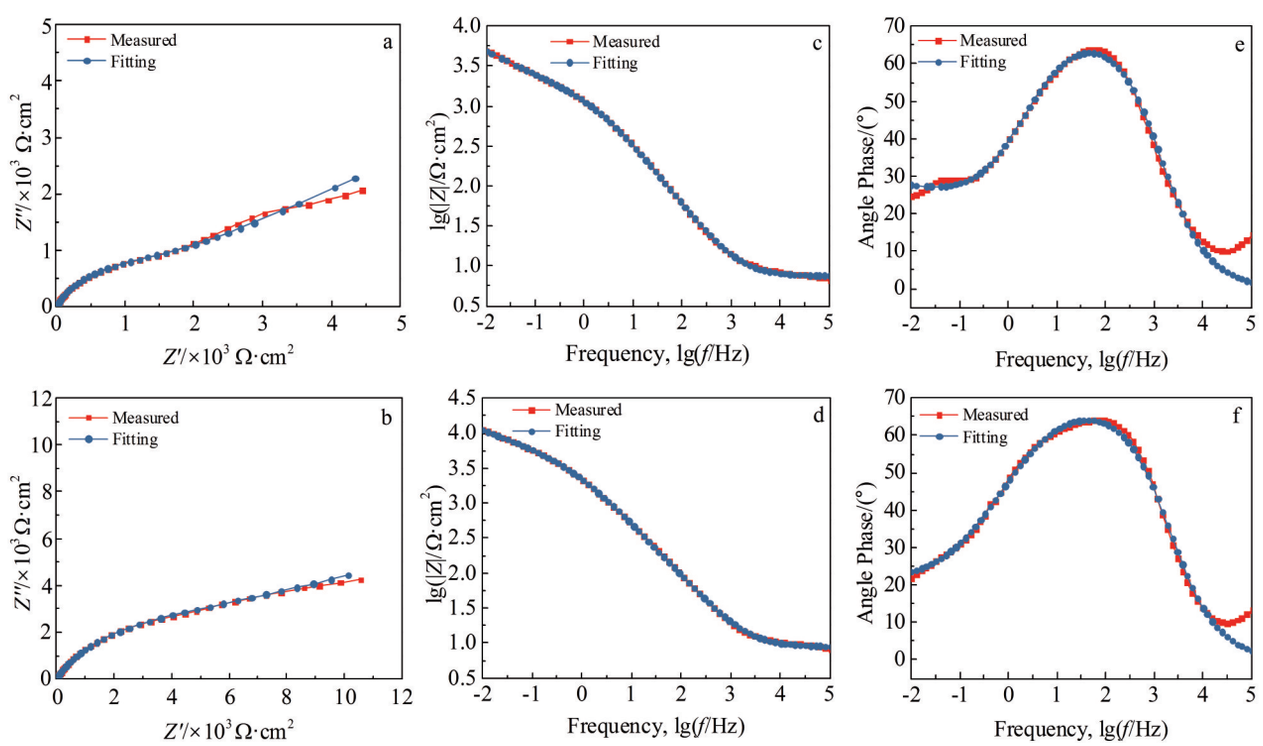

Fig.9 Simulated and measured Nyquist plots (a, b), impedance-frequency plots (c, d), and phase angle-frequency plots (e, f) of SLM pure Ti (a, c, e) and SLM+ECAP pure Ti (b, d, f) in Ringer's SBF

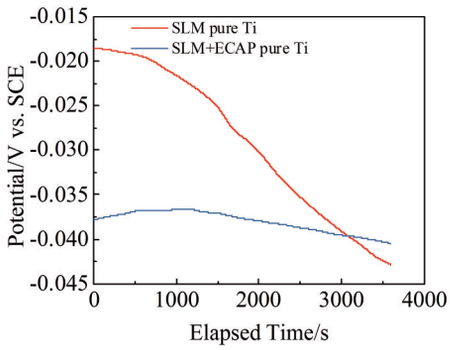

Fig.10 Open circuit potential curves of SLM pure Ti and SLM+ECAP pure Ti in simulated oral saliva

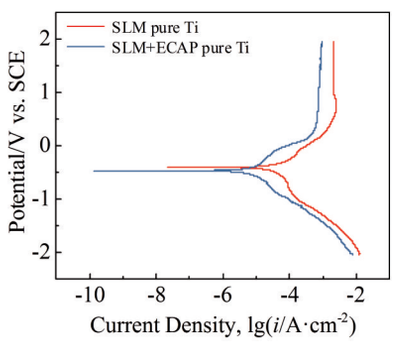

Fig.11 Potential polarization curves of SLM pure Ti and SLM+ECAP pure Ti in simulated oral saliva

oral saliva for 3600 s, which are similar to each other. The cathodic polarization dominates firstly. Then the electrode potential moves along the positive direction, and the current density decreases. With the positive shift of the electrode potential of about −0.48 V vs. SCE, the anodic polarization is in the dominated position for the pure SLM pure Ti and SLM+ECAP pure Ti. Then, the electrode potential continues to increase, and the current density also begins to increase. When the electrode potential increases to 0.3 V vs. SCE, the current density of SLM+ECAP pure Ti remains, indicating that the specimens enter the passivation zone and are at a stable corrosion state. When the electrode potential of SLM pure Ti increases to 0.85 V vs. SCE, the current density remains, indicating that SLM pure Ti enters the passivation zone. E_{corr} of the SLM+ECAP pure Ti is slightly lower than that of the SLM pure Ti. Besides, the more positive the corrosion potential, the better the corrosion resistance. The corrosion resistance of the pure Ti specimens should also be evaluated through i_{corr}, because i_{corr} reflects the dissolution process of materials, and the smaller the current density of the working electrode surface, the less the dissolution of materials, and therefore the better the corrosion resistance of materials. Table 6 shows the corrosion resistance properties of SLM pure Ti and SLM+ECAP pure Ti in simulated oral saliva. The E_{corr} value of SLM+ECAP pure Ti is slightly smaller than that of SLM pure Ti, but its i_{corr} is obviously small. The R_p value of SLM+ECAP pure Ti is large, which is more than four times higher than that of SLM pure Ti. Thus, it can be concluded that the corrosion rate of SLM+ECAP pure Ti is slower, the surface oxide film is more completed, and thereby the corrosion resistance is better, compared with those of SLM pure Ti.

Fig.12 shows the Nyquist plots and Bode plots of SLM pure Ti and SLM+ECAP pure Ti in simulated oral saliva. The capacitive arc radius of SLM+ECAP pure Ti is larger than that of SLM pure Ti, i.e., SLM+ECAP pure Ti has better corrosion resistance in the simulated oral saliva. Meanwhile, both SLM pure Ti and SLM+ECAP pure Ti have Warburg impedance in the corrosion process of the electrode. The absolute value of impedance of SLM+ECAP pure Ti is higher than that of SLM pure Ti, indicating that the corrosion resistance of pure Ti is enhanced by ECAP deformation treatment.

According to Fig.12c, the phase angle of SLM pure Ti and SLM+ECAP pure Ti at high frequency is approximately 15°. In the low frequency region, the phase angle of SLM+ECAP pure Ti is higher than that of SLM pure Ti, and the phase angle of either specimen cannot reach 90° during the whole process, indicating that neither of the two specimens exhibit pure capacitive response. It is found that the intermediate

Table 6 Corrosion resistance properties of SLM pure Ti and SLM+ECAP Ti specimens in simulated oral saliva

Specimen	E_{corr}/V vs. SCE	i_{corr}/×10^{-6} A·cm^{-2}	R_p/Ω·cm^2
SLM pure Ti	−0.413 22	9.686 7	1858.2
SLM+ECAP pure Ti	−0.474 07	2.043 2	8809.7

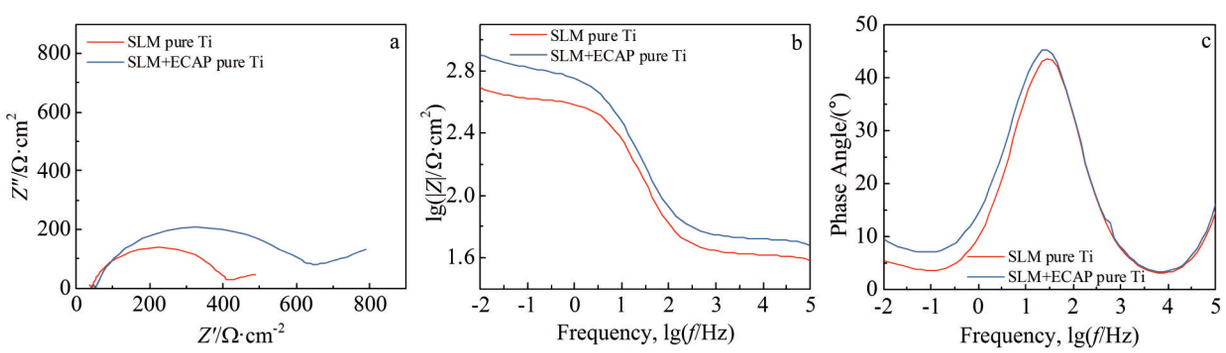

Fig.12 Nyquist plots (a), impedance-frequency plots (b), and phase angle-frequency plots (c) of SLM pure Ti and SLM+ECAP pure Ti in simulated oral saliva

frequency range of the SLM pure Ti is narrower than that of the SLM+ECAP pure Ti, and the maximum phase angle of the SLM+ECAP pure Ti is higher than that of the SLM pure Ti. Thus, it can be concluded that the charge transfer can hardly occur, the corrosion rate of the electrode is slow, and the better corrosion resistance of pure Ti is achieved.

The results of simulated EIS curves of the specimens in simulated oral saliva (Fig. 13) are consistent with those in the Ringer's SBF. The fitting results are shown in Table 7.

It can be seen from Table 7 that ECAP deformation has a great influence on the passive film of pure Ti surface, as indicated by the passive film resistance R_2 of the two specimens. The passive film resistance of SLM pure Ti and SLM+ECAP pure Ti is 358.5 and 528.9 $\Omega\cdot cm^2$, respectively. After ECAP deformation, the resistance of passive film is increased obviously. Meanwhile, the values of n and W_1 of SLM+ECAP pure Ti are also slightly increased, compared with those of SLM pure Ti, which leads to the decrease in the charge on the electrode surface and the corrosion rate. Therefore, the corrosion resistance of SLM+ECAP pure Ti is better than that of SLM pure Ti.

3 Discussion

After the plastic deformation, the change in grain size, the transformation of texture components, the variation of dislocation density and the defects can all affect the corrosion resistance properties of pure titanium. According to the polarization resistance R_p in Table 4 and Table 6, when the grain boundaries are increased, the polarization resistance of SLM+ECAP pure Ti is enhanced, and the corrosion can hardly occur. The main reason is that ECAP can introduce a large number of dislocations in the grains and at the grain boundaries, and the passive film can be formed from both the grain and the grain boundary, therefore improving the compactness of the passive film and hindering the penetration of substances into the passive film in the corrosive medium. In addition, the i_{corr} of SLM+ECAP pure Ti is much lower than that of SLM pure Ti, indicating that during the corrosion process, the self-repairing ability of passive film on the surface of SLM+ECAP pure Ti is stronger than that of SLM pure Ti due to the high energy storage in dislocations and grain boundaries of pure Ti after ECAP, which is beneficial to the formation and self-repairing of passive film. The passive film can hinder the further corrosion. After ECAP, the increased grain boundaries reduce the impurities and precipitations, thus improving the corrosion resistance of the pure Ti.

The type and strength of textures also affect the corrosion resistance of titanium. It can be seen from Fig. 3 that the {0002} crystal plane of SLM pure Ti forms a strong texture with an angle of about 65° from ND, while the orientation of formed texture in SLM+ECAP pure Ti is closer to ED and the texture rotates along ND with a small angle. The texture

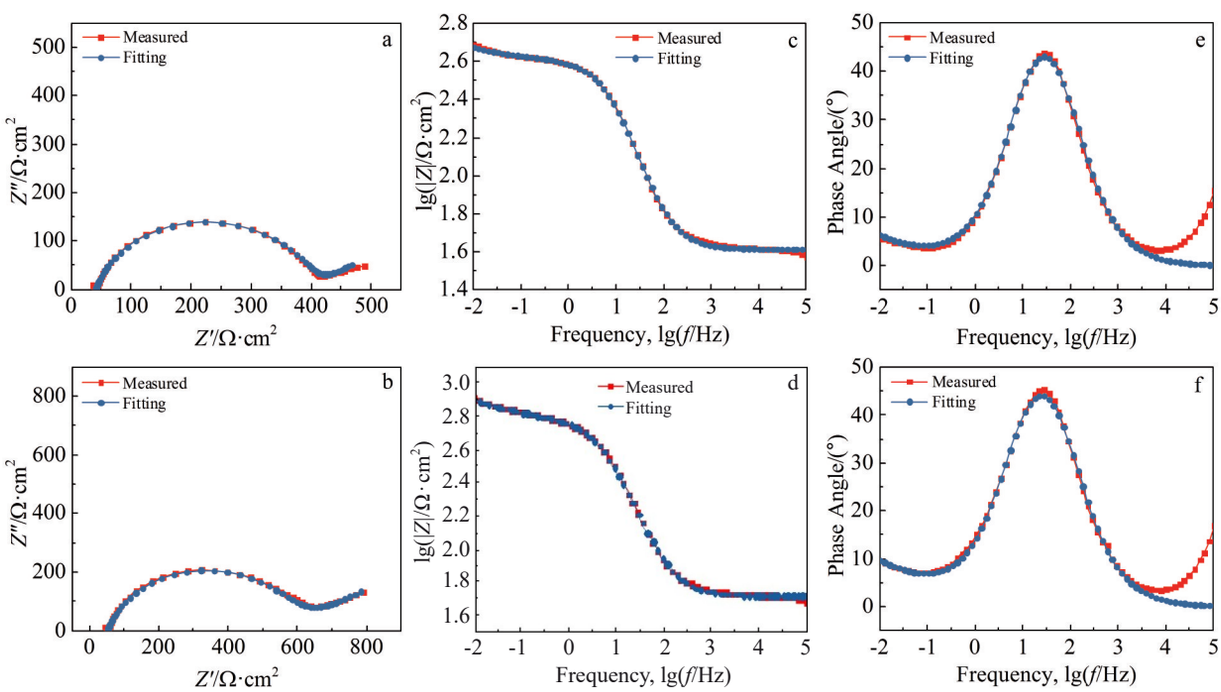

Fig.13 Simulated and measured Nyquist plots (a, b), impedance-frequency plots (c, d), and phase angle-frequency plots (e, f) of SLM pure Ti (a, c, e) and SLM+ECAP pure Ti (b, d, f) in simulated oral saliva

Table 7 Simulated EIS results of SLM pure Ti and SLM+ECAP pure Ti specimens in simulated oral saliva

Specimen	$R_1/\Omega\cdot cm^2$	$CPE_1/\times10^{-4}\ \Omega^{-1}\cdot cm^{-2}\cdot s^n$	n	$R_2/\Omega\cdot cm^2$	$W_1/\Omega^{-1}\cdot cm^{-2}\cdot s^{0.5}$
SLM pure Ti	40.98	1.177 9	0.813 51	358.5	0.355 69
SLM+ECAP pure Ti	51.67	1.021 8	0.829 95	528.9	0.394 72

strength of {0002} plane shows that the basal texture strength of SLM pure Ti is 6.10, and that of SLM+ECAP pure Ti is 8.57. Hoseini[22] and Gurao[23] et al obtained the ultrafine-grained pure titanium with different texture components through different paths of ECAP, and found that the texture can significantly improve the corrosion resistance of ultrafine-grained pure titanium. In addition, the texture has a more obvious effect on the corrosion resistance of specimens than the refinement treatment of crystallization does.

4 Conclusions

1) After equal channel angular pressing (ECAP), the grain boundaries and dislocation density of pure titanium prepared by selective laser melting (SLM) are increased. The preferred orientation of the polar figure of SLM+ECAP pure Ti is not obvious, but its polar density is increased.

2) In the corrosion environment of Ringer's simulated body fluid and simulated oral saliva, SLM+ECAP pure Ti has higher energy storage at dislocations and grain boundaries than SLM pure Ti does. Therefore, the self-repairing ability of passive film of SLM+ECAP pure Ti is better, i. e., the corrosion resistance of SLM+ECAP pure Ti is better.

3) The equivalent circuit fitting results of alternate current impedance spectrum show the accuracy of prediction.

References

1 Jiang L N, Eglantine C, Lilia K *et al*. *Materials Science and Engineering A*[J], 2013, 581: 8

2 Zhang Y, Figueiredo R B, Alhajeri S N *et al*. *Materials Science and Engineering A*[J], 2011, 528: 7708

3 Djavanroodi F, Ebrahimi M, Rajabifar B *et al*. *Materials Science and Engineering A*[J], 2010, 528: 745

4 Long F W, Jiang Q W, Xiao L *et al*. *Materials Transactions*[J], 2011, 52(8): 1617

5 Mughrabi H, Höppel H W. *International Journal of Fatigue*[J], 2010, 32(9): 1413

6 Collini L. *Procedia Engineering*[J], 2010, 2(1): 2065

7 Agapovichev A, Kokareva V, Smelov V *et al*. *IOP Conference Series: Materials Science and Engineering*[J], 2016, 156: 12 031

8 Zong Xuewen, Zhang Jian, Liu Wenjie *et al*. *Rare Metal Materials and Engineering*[J], 2021, 50(4): 1304 (in Chinese)

9 Cruz V, Chao Q, Birbilis N *et al*. *Corrosion Science*[J], 2019, 164: 108 314

10 Liu W J, Zong X W, Yang Y M *et al*. *Rare Metal Materials and Engineering*[J], 2020, 49(12): 4031

11 Li Z H, Li B Q, Bai P K *et al*. *Materials*[J], 2018, 11(7): 1172

12 Hou Yu, Geng Yaoxiang, Chen Jinhan *et al*. *Rare Metal Materials and Engineering*[J], 2020, 49(11): 3943 (in Chinese)

13 Sercombe T, Li X. *Materials Technology*[J], 2016, 31(2): 77

14 Wang Haojie, Yang Fang, Guo Zhimeng *et al*. *Rare Metal Materials and Engineering*[J], 2021, 50(2): 709 (in Chinese)

15 Sabelkin V, Cobb G, Shelton T *et al*. *Materials & Design*[J], 2019, 182: 108 095

16 Covarrubias E E, Eshraghi M. *JOM*[J], 2018, 70(3): 336

17 Wronski M, Wierzbanowski K, Wojtas D *et al*. *Metals and Materials International*[J], 2018, 24(4): 802

18 Balakrishnan A, Lee B C, Kim T N *et al*. *Trends Biomater Artif Organs*[J], 2008, 22(1): 58

19 Irfan O M, Al-Mufadi F A, Djavanroodi F. *Metallurgical and Materials Transactions A*[J], 2018, 49(11): 5695

20 GB/T 13810-2007[S], 2008

21 ASTM F67-2006a[S], 2013

22 Hoseini M, Shahryari A, Omanovic S *et al*. *Corrosion Science* [J], 2009, 51(12): 3064

23 Gurao N P, Manivasagam G, Govindaraj P *et al*. *Metallurgical and Materials Transactions A*[J], 2013, 44(12): 5602

ECAP对SLM纯钛组织及其耐腐蚀性能的影响

罗　雷[1,2]，段西明[1]，马炜杰[1]，杨西荣[1,2]，刘晓燕[1,2]，王敬忠[1,2]

(1. 西安建筑科技大学 冶金工程学院，陕西 西安 710055)

(2. 陕西省纳米材料与技术重点实验室，陕西 西安 710055)

摘　要：为了提高纯钛在林格氏模拟体液和模拟口腔唾液环境中的耐腐蚀性能，采用等通道转角挤压（ECAP）技术对激光选区熔化（SLM）技术制备的商业纯钛进行改性处理。通过透射电子显微镜和电子背向散射衍射技术对SLM纯钛和SLM+ECAP纯钛进行组织检测，并在三电极体系下进行耐腐蚀性能的测试。结果表明：SLM+ECAP纯钛比SLM纯钛试样的晶粒尺寸小，晶界多，位错密度增大，极图的择优取向不太明显，但极密度有所增加。在林格氏模拟体液和模拟口腔唾液环境中，SLM+ECAP纯钛比SLM纯钛的自腐蚀电流密度小，极化电阻大，阻抗半径大。采用ZSimpWin软件对交流阻抗谱进行等效电路拟合，拟合结果和实验测量数据较为吻合。SLM+ECAP纯钛的耐腐蚀性能比SLM纯钛好。

关键词：等通道转角挤压；激光选区熔化；纯钛；耐腐蚀性能

作者简介：罗　雷，男，1985年生，博士，副教授，西安建筑科技大学冶金工程学院，陕西 西安 710055，E-mail：luolei@xauat.edu.cn